Polym. Bull. (2010) 64:483–495
DOI 10.1007/s00289-009-0216-y

ORIGINAL PAPER

Deformation of dispersed PA66 phase in drawn PA66/SAN blend

Wenjing Li · Alois K. Schlarb · Martin Weber · Michael Evstatiev

Received: 29 April 2009 / Revised: 9 November 2009 / Accepted: 21 November 2009 /
Published online: 2 December 2009

Abstract Polyamide 66/styrene acrylonitrile (PA66/SAN) drawn strands were prepared by stretching the corresponding extrudates at 130 °C. During stretching, the PA66 droplets in the extrudate are deformed as a result of the stretching-induced stress. In drawn strands, the morphology of the deformed PA66 is greatly affected by the morphology of the PA66 dispersed phase in the extrudate as well as by the interfacial adhesion between the PA66 and SAN matrix. Upon stretching, the cylindrical PA66 threads in the uncompatibilized extrudate [styrene acrylonitrile maleic anhydride (SANMA) as compatibilizer] deform into PA66 fibrils with large aspect ratio, while the small spherical PA66 droplets are only slightly deformed. Interfacial adhesion between the PA66 and SAN is improved in the compatibilized PA66/SAN extrudate. Consequently, despite the small diameter, PA66 droplets in the compatibilized blend are greatly deformed during stretching.

Keywords Blend · Morphology · Deformation · Fibrils

W. Li (✉)
Institut für Verbundwerkstoffe (Institute for Composite Materials), University of Kaiserslautern, Erwin Schrödinger Str., 67663 Kaiserslautern, Germany
e-mail: wenjing.li@ivw.uni-kl.de

A. K. Schlarb
Chair of Composite Engineering, University of Kaiserslautern, Gottlieb Daimler Strasse, Gebäude 44, 67663 Kaiserslautern, Germany
e-mail: alois.schlarb@mv.uni-kl.de

M. Weber
BASF SE, Polymer Research Division, Engineering Plastics GKT/B – B1, Carl-Bosch-Str. 38, 67056 Ludwigshafen, Germany

M. Evstatiev
Laboratory on Polymers, Sofia University, 1126 Sofia, Bulgaria

Introduction

Blending of polymers is an effective route to obtain new materials with improved properties. Since most of the polymers are immiscible, thus a decrease of mechanical properties is usually observed. Processing of an incompatible polymer blend in which the dispersed phase forms in situ reinforced fibers is the preferable way to achieve the highest mechanical properties. In order to obtain such structure, the so called microfibrillar composites (MFC) were developed [1–3]. Preparation of MFC includes three basic steps: (1) melt blending of two polymers with different melting temperatures, (2) drawing of the extrudate for a good orientation of the two phases, (3) thermal treatment at a temperature between the melting temperatures of the two polymers. Several blend combinations were selected for preparing MFC, among which polyethylene terephthalate (PET)/polyolefin received special attention. It was reported that PET microfibrils with large aspect ratio can be generated by stretching the extrudate at about 80 °C [4, 5].

Demonstrating superior toughness and tensile properties, polyamide 66 (PA66) is widely used as engineering material. Polyamide fibers show even higher tensile properties, such as PA66 textile fibers whose tensile strength reaches as high as 3000 MPa. Demonstrating outstanding tensile properties, polyamide fibers are considered as potential candidates for reinforcing polymer matrices. Numerous investigations on MFC showed that polymer fibrils with high aspect ratio can be generated by stretching of the polymer blends above the glass-transition temperatures. Evstatiev et al. [5] investigated the PA66/PA6 and PET/PA6/PA66 MFC, however, due to the miscibility of the two polyamides, separate PA6 or PA66 microfibrils are not observed. Pesneau blended PA6 with polypropylene (PP) using a twin-screw extruder, polypropylene-grafted maleic anhydride (PP-g-MA) was used as compatibilizer for the two polymers. The extrudate was drawn while the two polymers were still in molten state. It was reported that PA6 fibrils were obtained in both uncompatibilized and compatibilized drawn strands [6]. PA66/PP MFC was studied by Huang et al. [7]. The cited author reported that the increase in the viscosity ratio between PA66 and PP is favorable for the fibrillization of PA66, while the elevation in the concentration of PP-g-MA is unfavorable for the fibrillization.

The morphology of fibrils in drawn strands is affected by the blend composition [8, 9], stretching ratio [10–12], the incorporation of compatibilizer [13], and the viscosity ratio between the reinforcement component and the matrix [14, 15]. In this study, PA66 and SAN are selected as the polymer pair for preparing MFC, PA66 is expected to act as the reinforcement in the SAN matrix. SAN is known as a rigid amorphous polymer, its glass-transition temperature (T_g) is above 100 °C. The blend of interest here has a matrix that is generally brittle (SAN) and a dispersed phase that is usually ductile. Two types of SAN with different viscosities were selected as polymer matrix for the preparation of PA66/SAN MFC. In order to modify the interfacial adhesion between PA 66 and SAN, styrene acrylonitrile maleic anhydride (SANMA) terpolymers were used as additive. From numerous studies it is known that during the melt blending, SANMA reacts with PA, thus leading to the formation of styrene-acrylonitrile-grafted polyamide (SAN-g-PA)

which acts as a perfect compatibilizer between PA66 and SAN [16–19]. The purpose of this study is to explore the effects of viscosity ratio and compatibilizer on the morphology and properties of PA66/SAN drawn strands.

Experimental

Materials

PA66 (Utramid® A4401) and two types of SAN with different viscosities (SAN-HV and SAN-LV) as well as a compatibilizer SANMA were provided by BASF SE (Ludwigshafen, Germany). All important properties of theses products are summarized in Table 1. The number average molecular weight of SANMA was 60.000 g/mol such that on average, approximately 12 maleic anhydride groups were randomly distributed within the SANMA chain.

Sample preparation

Prior to processing, all the materials were dried for 12 h at 80 °C to avoid hydrolytic degradation during melt processing. Uncompatibilized and compatibilized PA66/SAN blends with the weight ratio of 30/70 were extruded with a co-rotating twin-screw extruder (Brabender PL2000, Brabender GmbH & Co. KG Duisburg, Germany). The diameter of the screw was 25 mm and the L/D (length/diameter ratio) was 22. The temperatures from the hopper to the die were set at 230, 270, 270, 275, 275 °C. After coming out of the extruder (2-mm capillary die), the extrudate was immediately quenched in a water bath at 90 °C. After passing through the take-up device, the bristle was heated up to 130 °C in a hot air chamber and subsequently drawn by a stretching device as described in Fig. 1. The draw ratio which is defined as the ratio between the speed of stretching device and the speed of the take-up device was always kept at 5. The designation and composition of the materials are given in Table 2.

Characterization

The extrudates and drawn strands were etched in tetrahydrofuran (THF) for 24 h at ambient temperature to remove SAN. The etched and unetched extrudates and drawn strands were inspected in a scanning electron microscope (JEOL JSM-6300,

Table 1 Properties of the materials

Materials	Composition (wt%)	T_g (°C)	Viscosity number (mL/g)[a]
SAN-LV	Styrene/acrylonitrile (75/25)	111	65
SAN-HV	Styrene/acrylonitrile (75/25)	112	80
SANMA	Styrene/acrylonitrile/maleic anhydride (74/24/2)	112	66

[a] Determined in DMF (0.5 wt% solution, 25 °C)

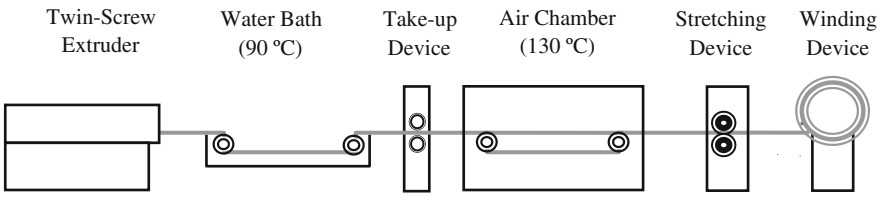

Fig. 1 Schematic illustration of the experimental setup for stretching the extrudate

Table 2 Material designation and composition

Designation	Composition	Parts (wt%)
PA/SAN-HV	PA66/SAN-HV	30/70
PA/SAN-LV	PA66/SAN-LV	30/70
PA/SAN-HV/0.5MA	PA66/SAN-HV/SANMA	30/69.5/0.5
PA/SAN-HV/3MA	PA66/SAN-HV/SANMA	30/67/3

Tokyo, Japan) operating at an accelerate voltage of 25 kV. All the specimens were coated with a thin gold layer prior to SEM analysis. The number average diameters (D_n) of PA66 droplets in the PA/SAN-LV, PA/SAN-HV/0.5MA, and PA/SAN-HV/3MA extrudates were determined by analyzing the SEM images using the following equation:

$$D_n = \frac{\sum_i N_i D_i}{\sum_i N_i} \quad (1)$$

D_i is the diameter of each droplet and N_i is the number of droplets with the diameter D_i.

Disks of PA66 and SAN were pressed at 275 °C. The apparent viscosity of the polymers was measured as a function of apparent shear rate at 275 °C using a Rheometrics ARES rheometer (Rheometric Scientific, NJ, USA). All the tests were performed in the frequency mode.

Dynamic mechanical characterization was performed using a Gabo EPLEXOR 100-N dynamic mechanical analyzer (GABO QUALIMETER Testanlagen GmbH, Ahlden, Germany) with a tensile mode. The samples were measured from 0 to 160 °C at a frequency of 10 Hz with a heating rate of 2 °C/min. The storage modulus and tan δ were recorded as a function of temperature.

Tensile strength of the drawn strands was measured by Zwick 1474 machine (Ulm, Germany) at room temperature with a crosshead speed of 5 mm/min. Special clamps were used to avoid the damage of the drawn strands. All the data presented correspond to the average of five measurements.

Results and discussion

Morphology of PA66 in extrudates

Figure 2 shows the morphology of the PA66 dispersed phase in the extrudates. The PA66 droplet size is strongly affected by the type of SAN and the incorporation of

SANMA as compatibilizer. In the PA/SAN-HV extrudate, the PA66 droplets are noticeably larger than those in the PA/SAN-LV extrudate (Fig. 2a, b). More interestingly, most of the PA66 droplets in the PA/SAN-HV extrudate deform into cylindrical threads, while in the PA/SAN-LV extrudate only a small amount of PA66 droplets are deformed. As shown in Fig. 2c and d, incorporation of SANMA as compatibilizer greatly decreases the droplet size of PA66, and the size decreases more with increasing content of SANMA. The number average diameters of PA66 droplets in the PA/SAN-LV, PA/SAN-HV/0.5MA, and PA/SAN-HV/3MA extrudates are listed in Table 3.

During melt extrusion the size and shape of dispersed phase are mainly controlled by interfacial tension, rheological properties and the complex strain field of the extruder [20]. Deformation of a droplet is dependent on two governing factors: the viscosity ratio between the dispersed phase and the continuous phase

$$\lambda = \frac{\eta_{\mathrm{d}}}{\eta_{\mathrm{m}}} \tag{2}$$

and the Weber number

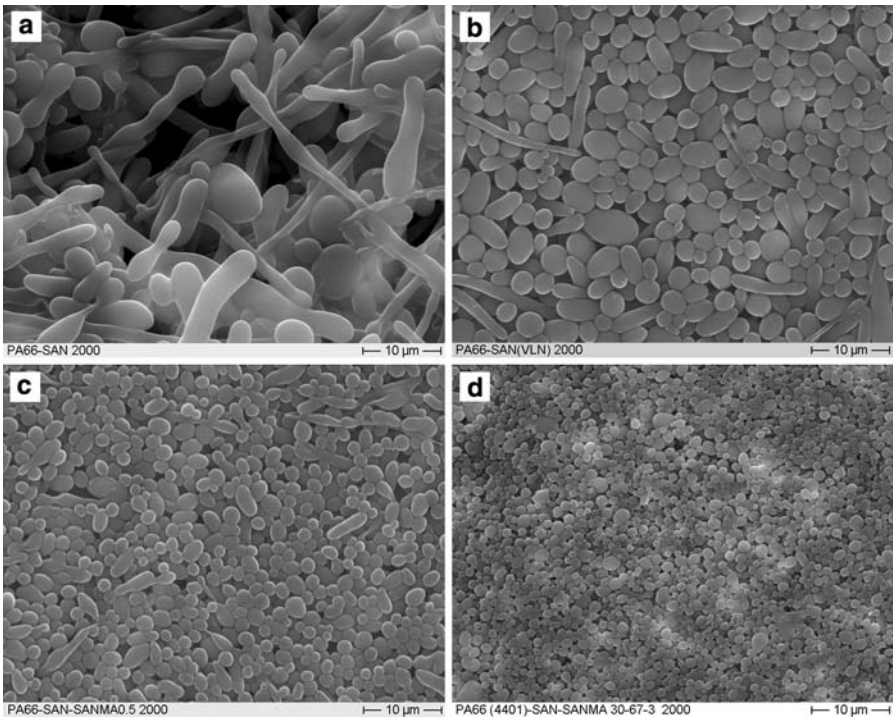

Fig. 2 Morphology of PA66 dispersed phase in the etched extrudates (by THF): **a** PA/SAN-HV, **b** PA/SAN-LV, **c** PA/SAN-HV/0.5MA, **d** PA/SAN-HV/3MA

Table 3 Number average diameter (D_n) of PA66 droplets in PA/SAN-LV, PA/SAN-HV/0.5MA, and PA/SAN-HV/3MA extrudates

Extrudate	D_n of PA66 (μm)
PA/SAN-LV	4.2 ± 1.7
PA/SAN-HV/0.5MA	2.7 ± 0.6
PA/SAN-HV/3MA	<1.0

$$W_e = \frac{\eta_m \gamma R}{\sigma} \tag{3}$$

which is the ratio between the deforming stress $\eta_m\gamma$ (matrix viscosity times shear rate imposed by the flow) and the interfacial force σ/R. σ is the interfacial tension between the two phases and R is the radius of the droplet [21, 22]. Deformation of droplets is known to increase with increasing W_e. If W_e exceeds a critical value which is known as the critical Weber number, $(W_e)_c$, the droplet will deform and even break [22–24]. According to Wu [20], for a viscoelastic droplet, the correlation between the critical Weber number $(W_e)_c$ and the viscosity ratio is given by Eq. 4.

$$(W_e)_c = 4\lambda^{\pm 0.84} \tag{4}$$

The plus (+) sign applies for $\lambda > 1$, and minus (−) sign for $\lambda < 1$. This empirical relationship is widely adopted for explaining droplet deformation and break up in polymer blends [25–28]. If $\lambda > 1$, the $(W_e)_c$ becomes higher with increasing λ. Consequently the W_e of a polymer blend is less likely to exceed the $(W_e)_c$, and an increase in droplet size is usually observed with increasing λ [20, 25, 27].

With the present blend system, however, an opposite trend is noticed. The viscosities versus shear rate for PA66, SAN-HV, and SAN-LV are plotted in Fig. 3. For PA/SAN-HV and PA/SAN-LV extrudates, the $\lambda_{PA/SAN\text{-}HV}$ and $\lambda_{PA/SAN\text{-}LV}$ are >1 since the viscosity of PA66 is much higher than that of the SAN in the whole

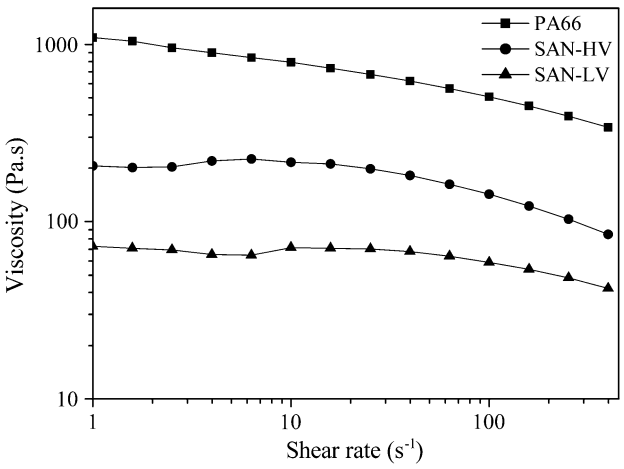

Fig. 3 Viscosities of PA66, SAN-HV, and SAN-LV

shear rate range. The $\lambda_{PA/SAN\text{-}LV}$ is even higher than the $\lambda_{PA/SAN\text{-}HV}$ as the viscosity of SAN-LV is much lower than that of the SAN-HV. According to Eq. 4, the $(W_e)_c$ for PA/SAN-LV blend is higher than that for the PA/SAN-HV. Therefore, the PA66 droplets in the PA/SAN-LV extrudate should be larger or at least more deformed than those in the PA/SAN-HV extrudate. However, the experimental result shows that the PA66 droplets in PA/SAN-HV extrudate are of larger diameter, which indicates that the "viscosity ratio and Weber number" theory is not applicable to our blend system. In fact, there are several factors which may influence the deformation of droplets: flow type and flow intensity, viscosity ratio, elasticity of polymers, composition, thermodynamic interactions, time, etc. There is no theory able to describe the deformability of viscoelastic droplet suspended in a viscoelastic or even Newtonian medium. In addition, the effect of droplets coalescence on the final morphology should also be taken into consideration [29].

Compatibilizer is known to be able to increase the degree of dispersion and stabilize the morphology of polymer blends [30]. In the PA/SAN-HV/0.5MA and PA/SAN-HV/3MA extrudates, SAN-g-PA66 copolymers are in situ formed via the anhydride/amino reaction. The interfacial tension between PA66 and SAN is thereby greatly decreased and smaller droplet size is achieved.

Morphology of PA66 in drawn strands

The drawn strands were etched by THF, and the SAN was removed. Figure 4 shows the morphology of the remaining PA66 phase in the drawn strands. After stretching, PA66 droplets in the PA/SAN-HV extrudate deform into long fibrils (Fig. 4a). Large magnification SEM image shows that the average diameter of the PA66 fibrils is about 0.4 μm (Fig. 4b). However, the aspect ratio of these fibrils is difficult to estimate as the length of the fibrils is unknown. In the PA/SAN-LV drawn strands, some PA66 fibrils are observed, the diameter is less than 1 μm; however, most of the PA66 droplets remain in spherical shape (Fig. 4c). A similar morphology is observed for the etched PA/SAN-HV/0.5MA drawn strand (Fig. 4d). For the PA/SAN-HV/3MA drawn strand, numbers of greatly deformed PA66 droplets are observed (Fig. 4e). However, these deformed PA66 droplets cannot be defined as fibrils due to the low aspect ratio, since both ends of the deformed droplets are usually observed.

Stretching of PA66/SAN blends was carried out in hot air chamber at around 130 °C. At this temperature, as seen in Fig. 5 representing storage modulus versus temperature, the storage modulus of PA66 is much higher than that of SAN. Based on the difference in storage modulus, the stretching-induced stress breaks the weak adhesion between PA66 droplets and SAN, cracks are thereby initiated [31]. It is probable that decohesion first starts along the stretching direction at the droplet tips. For the PA/SAN-LV extrudate, the crack can easily propagate at the interface due to the weak interfacial adhesion and the low contact area between the PA66 droplets and SAN matrix. Therefore, a total detachment between the PA66 droplets and SAN matrix takes place, and large voids are observed (Fig. 6a). In the PA/SAN-HV extrudate it is known that the PA66 droplets deform into cylindrical threads. The stretching-induced stress can be effectively transferred to the PA66 threads because

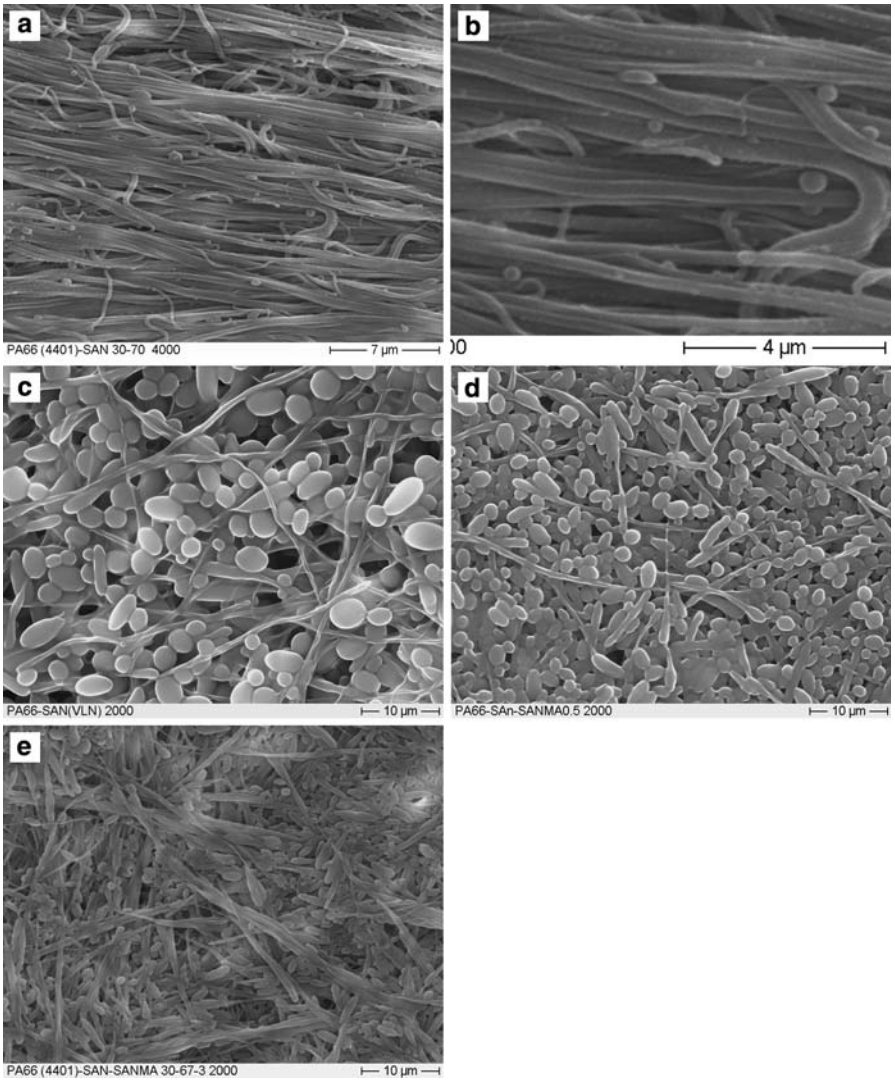

Fig. 4 Morphology of PA66 dispersed phase in the etched drawn strands (by THF): **a** PA/SAN-HV, **b** PA/SAN-HV at large magnification, **c** PA/SAN-LV, **d** PA/SAN-HV/0.5MA, **e** PA/SAN-HV/3MA

of the increased contact area, thus resulting in further deformation of PA66 droplets, consequently the PA66 fibrils are observed (Fig. 6b). In the etched PA/SAN-LV drawn strand, some PA66 fibrils are also noticed. These fibrils are believed to be originated from the deformed PA66 droplets in the extrudate (Fig. 2b).

In the etched PA/SAN-HV/0.5MA drawn strand, numbers of PA66 droplets remain undeformed, which indicates that debonding between PA66 droplets and SAN matrix still takes place during stretching. At high loading of SANMA (3 wt%), as seen in Fig. 7a, the interface between PA66 droplets and SAN cannot be easily distinguished, and better interfacial adhesion between PA66 droplets and SAN

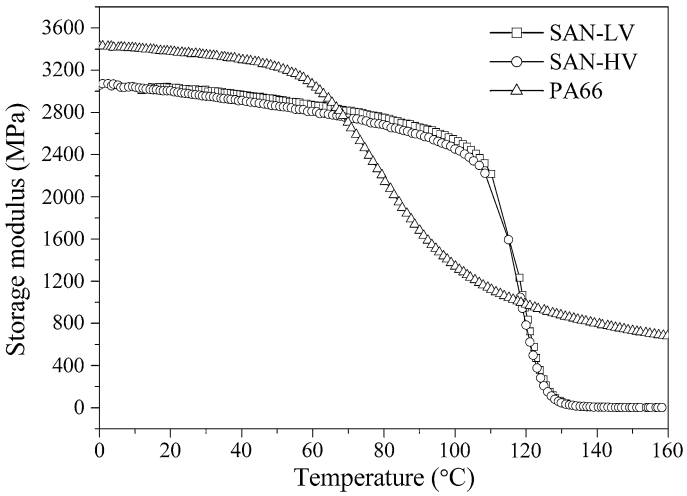

Fig. 5 Thermal dynamic curves of PA66, SAN-HV, and SAN-LV

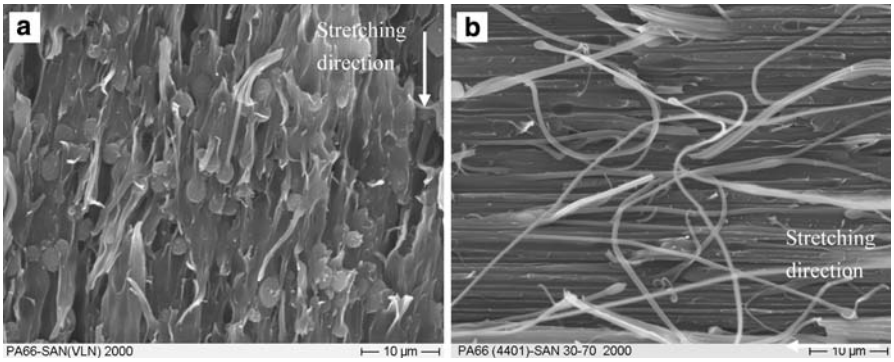

Fig. 6 Morphology of **a** PA/SAN-LV and **b** PA/SAN-HV drawn strands

matrix is achieved when compared with the uncompatibilized blend (Fig. 7b). The improved interfacial adhesion promotes stress transfer to the PA66 droplets during stretching, consequently despite the small diameter, most of the PA66 droplets are greatly deformed (but not deformed into PA66 fibrils).

As a summary, the stretching-induced deformation of PA66 droplets is schematically shown in Fig. 8. In the PA66/SAN-HV extrudate, upon stretching, the cylindrical PA66 threads in the extrudate deform into fibrils. While in the PA66/SAN-LV extrudate, the small spherical PA66 droplets are only slightly deformed. In the compatibilized PA66/SAN-HV extrudate, the formed SAN-g-PA66 copolymer at the interface improves the interfacial adhesion between PA66 and SAN-HV, thus facilitates the deformation of PA66 droplets. Consequently, the PA66 droplets are more deformed than those in the PA66/SAN-LV extrudate although the diameter is even smaller.

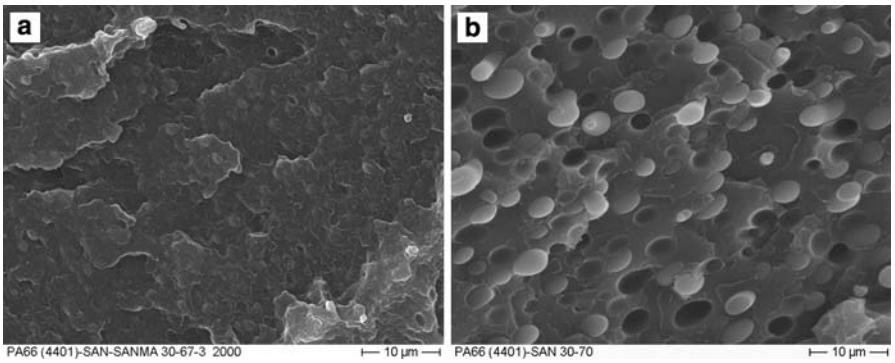

Fig. 7 Fracture surfaces of **a** PA/SAN-HV/3MA and **b** PA/SAN-HV extrudates

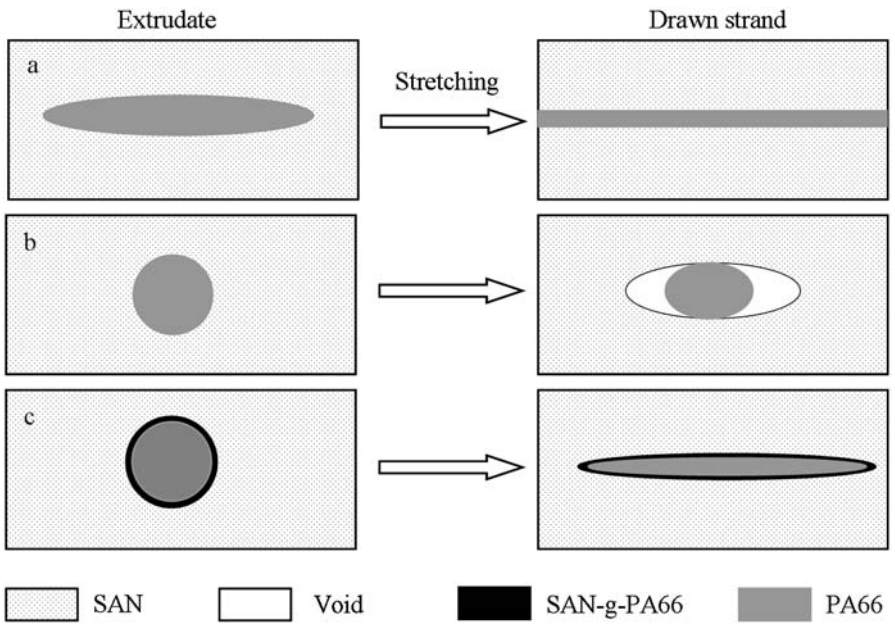

Fig. 8 Schematic of stretching-induced deformation of PA66 dispersed phase: **a** deformation of cylindrical PA66 threads in PA/SAN-HV extrudate, **b** deformation of small spherical PA66 droplets in PA/SAN-LV extrudate, **c** deformation of spherical PA66 droplets in PA/SAN-HV/3MA extrudate

Tensile strength of drawn strands

The tensile strength of PA66/SAN drawn strands is greatly dependent on structures of drawn strands. Due to the uniaxial alignment of PA66 fibrils, the reinforcement effect of PA66 fibrils is observed for PA/SAN-HV drawn strands, its tensile strength reaches as high as 160 MPa (Fig. 9). For PA/SAN-LV, PA/SAN-HV/0.5MA, and PA/SAN-HV/3MA drawn strands the reinforcement effect of PA66 fibril is less

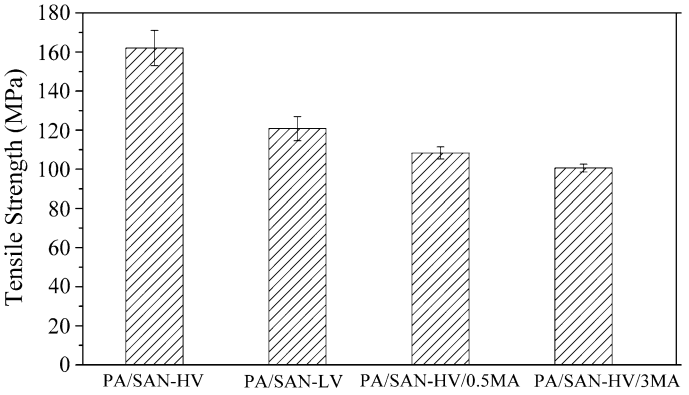

Fig. 9 Tensile strength of drawn strands

profound, since few fibrils are observed. In addition, the stretching-induced voids in these drawn strands deteriorate the tensile strength. Therefore, lower tensile strength is noticed for these three types of drawn strands.

Conclusions

The morphology of dispersed PA66 phase in PA66/SAN extrudates and drawn strands was investigated. In the PA/SAN-HV extrudate, the PA66 droplets exhibit large diameters; in addition, a great numbers of cylindrical PA66 threads are observed. Upon addition of SANMA as compatibilizer, the droplet size of PA66 is greatly decreased, at the same time, the interfacial adhesion between the dispersed PA66 phase and SAN matrix is improved.

During stretching, the dispersed PA66 phase is subjected to the stretching-induced stress. Compared with the PA66 droplets, upon stretching the cylindrical PA66 threads are easily deformed into fibrils due to the large contact area between the PA66 and SAN which promotes stress transfer. Therefore in the PA/SAN-HV drawn strand, PA66 fibrils with large aspect ratio are observed. During stretching of the compatibilized PA66/SAN drawn strand, the improved interfacial adhesion also enhances stress transfer, however, the dispersed PA66 droplets are too small to deform into fibrils.

Acknowledgment This work was finished in the frame of RLP Graduate School of Excellence and additionally supported by BASF SE.

References

1. Evstatiev M, Fakirov S (1992) Microfibrillar reinforcement of polymer blends. Polymer 33:877–880
2. Fakirov S, Evstatiev M, Schultz JM (1993) Microfibrillar reinforced composite from drawn poly(ethylene terephthalate)/nylon-6 blend. Polymer 34:4669–4679

3. Fakirov S, Evstatiev M, Petrovich S (1993) Microfibrillar reinforced composites from binary and ternary blends of polyesters and nylon 6. Macromolecules 26:5219–5226
4. Friedrich K, Evstatiev M, Fakirov S, Evstatie O, Ishii M, Harrass M (2005) Microfibrillar reinforced composites from PET/PP blends: processing, morphology and mechanical properties. Compos Sci Technol 65:107–116
5. Evstatiev M, Schultz JM, Petrovich S, Georgiev G, Fakirov S, Friedrich K (1998) In situ polymer/polymer composites from poly(ethylene terephthalate), polyamide-6, and polyamide-66 blends. J Appl Polym Sci 67:723–737
6. Pesneau I, Ait Kadi A, Bousmina M, Ph Cassagnau, Michel A (2002) From polymer blends to in situ polymer/polymer composites: morphology control and mechanical properties. Polym Eng Sci 42:1990–2004
7. Huang W, Shen J, Chen X, Chen H (2003) Factors influencing the fiberization and mechanical properties of polypropylene/polyamide 66 in situ composites. Polym Int 52:1131–1135
8. Quan H, Zhong GJ, Li ZM, Yang MB, Xie BH (2005) Morphology and mechanical properties of poly(phenylene sulfide)/isotactic polypropylene in situ microfibrillar blends. Polym Eng Sci 45:1303–1311
9. Xu HS, Li ZM, Wang SJ, Yang MB (2007) Rheological behavior of PET/HDPE in situ microfibrillar blends: influence of microfibrils' flexibility. J Polym Sci B 45:1205–1216
10. Li ZM, Yang MB, Xie BH, Feng JM (2003) In situ microfiber reinforced composite based on PET and PE via slit die extrusion and hot stretching: Influences of hot stretching ratio on morphology and tensile properties at a fixed composition. Polym Eng Sci 43:615–628
11. Li ZM, Yang W, Xie BH, Shen KZ, Huang R, Yang MB (2003) Morphology and tensile strength prediction of in situ microfibrillar poly(ethylene terephthalate)/polyethylene blends fabricated via slit-die extrusion-hot stretching-quenching. Macromol Mater Eng 289:349–354
12. Monticciolo A, Cassagnau P, Michel A (1998) Fibrillar morphology development of PE/PBT blends: rheology and solvent permeability. Polym Eng Sci 38:1882–1889
13. Fakirov S, Bhattacharyya D, Lin RJT, Fuchs C, Friedrich K (2007) Contribution of coalescence to microfibril formation in polymer blends during cold drawing. J Macromol Sci B 46:183–194
14. Lin XD, Cheung WL (2003) Study of poly(ethylene terephthalate)/polypropylene microfibrillar composites. I. Morphological development in melt extrusion. J Appl Polym Sci 89:1743–1752
15. Feng M, Gong F, Zhao C, Chen G, Zhang S, Yang M (2004) Effect of clay on the morphology of blends of poly(propylene) and polyamide 6/clay nanocomposites. Polym Int 53:1529–1537
16. Triacca VJ, Ziaee S, Barlow JW, Keskkula H, Paul DR (1991) Reactive compatibilization of blends of nylon 6 and ABS materials. Polymer 32:1401–1413
17. Majundar B, Kesskula H, Paul DR, Harvey NG (1994) Control of the morphology of polyamide/styrene-acrylonitrile copolymer blends via reactive compatibilizers. Polymer 35:4263–4279
18. Jafari SH, Poetschke P, Stephan M, Warth H, Alberts H (2002) Multicomponent blends based on polyamide 6 and styrenic polymers: morphology and melt rheology. Polymer 43:6985–6992
19. Weber M, Heckmann W, Goeldel A (2006) Styrenics/polyamide blends-reactive blending and properties. Macromol Symp 233:1–10
20. Wu S (1987) Formation of dispersed phase in incompatible polymer interfacial and rheological effects. Polym Eng Sci 27:335–343
21. Lazo NDB, Scott CE (2001) Morphology development during phase inversion in isothermal, model experiments: steady simple-shear and quiescent flow fields. Polymer 42:4219–4231
22. Puyvelde PV, Velankar S, Moldenaers P (2001) Rheology and morphology of compatibilized polymer blends. Curr Opin Colloid Interf 6:457–463
23. Favis BD, Chalifoux JP (1987) The effect of viscosity ratio on the morphology of polypropylene/polycarbonate blends during processing. Polym Eng Sci 27:1591–1600
24. Fortelny I, Kamenicka D, Kovar J (1988) Effect of the viscosity of components on the phase structure and impact strength of polypropylene/ethylene-propylene elastomer blends. Angew Makromol Chem 164:125–141
25. Everaert V, Aerts L, Groeninckx G (1999) Phase morphology development in immiscible PP/(PS/PPE) blends influence of the melt-viscosity ratio and blend composition. Polymer 40:6627–6644
26. Cassagnau P, Nietsch T, Bert M, Michel A (1998) Reactive blending by in situ polymerization of the dispersed phase. Polymer 40:131–138
27. Heino MT, Hietaoja PT, Vainio TP, Seppälä JV (1994) Effect of viscosity ratio and processing conditions on the morphology of blends of liquid crystalline polymer and polypropylene. J Appl Polym Sci 51:259–270

28. Hietaoja PT, Holsti-Miettinen RM, Seppälä JV, Ikkala OT (1994) The effect of viscosity ratio on the phase inversion of polyamide 66/polypropylene blends. J Appl Polym Sci 54:1613–1623
29. Utracki LA, Shi ZH (1992) Development of polymer blend morphology during compounding in a twin-Screw extruder. Part I: droplet dispersion and coalescence-a review. Polym Eng Sci 32:1824–1833
30. Koning C, Van Duin M, Pagnoulle C, Jerome R (1998) Strategies for compatibilization of polymer blends. Prog Polym Sci 23:707–757
31. Bai S, G'Sell C, Hiver J, Mathieu C (2005) Polypropylene/polyamide 6/polyethylene-octene elastomer blends. Part 3. Mechanisms of volume dilatation during plastic deformation under uniaxial tension. Polymer 46:6437–6446